HYDRODYNAMICS AND SEDIMENT DYNAMICS IN AN ICE-COVERED TIDAL FLAT

URS NEUMEIER[1], COLETTE CHENG[2]

1. *Institut des sciences de la mer de Rimouski, Université du Québec à Rimouski, 310 allée des Ursulines, Rimouski QC G5L 3A1, Canada.* urs_neumeier@uqar.ca.
2. *Institut des sciences de la mer de Rimouski, Université du Québec à Rimouski, 310 allée des Ursulines, Rimouski QC G5L 3A1, Canada.* colettechg@gmail.com.

Abstract: Land-fast ice changes hydrodynamics and sediment dynamics in the intertidal zones of the St. Lawrence Estuary during several months in winter. Currents were measured with four current meters and two current profilers on a shore-normal transect from low marsh to sandflat. The temporal and lateral current variations correspond to the usual intertidal pattern, except the strongest first flood current when water is pushed with high pressure under the ice still resting on the ground. Velocity profiles show currents decreasing downward near the bed, but also upward near the water-ice interface, which reduces the total flow and pushes the velocity maximum toward the bed. Suspended sediment concentration was higher on the low marsh compared to the tidal flat, probably because the finer low-marsh sediments were not protected by vegetation and they could be more easily resuspended than in summer.

Introduction

Subarctic areas like the St. Lawrence Estuary are characterized by several months of sea ice in winter, which attenuates waves and protects the shoreline from erosion (Troude and Sérodes 1988; Barnhart et al. 2014). Summer coastal processes in the St. Lawrence Estuary are relatively similar to the ones in temperate climates (Coulombier et al. 2012). However, sediment dynamics in marshes and tidal flats are dominated by winter processes, when sea ice transports sediments of all grain-sizes by ice rafting (Troude and Sérodes 1988; Neumeier 2011).

In the upper intertidal zone (approximately the high marsh zone), the ice foot is firmly attached to the ground during the whole winter. Seaward, land-fast ice move up and down with the tides; but horizontal movement is very limited as it is attached to the shore. In the intertidal zone, land-fast ice changes hydrodynamics, by constricting the space available for water flow, and by dissipating wave energy. In addition, land-fast ice mows most of the above-ground marsh vegetation, removing the canopy that protects marsh sediment and modifying bed roughness.

Neumeier, U., Cheng, C., 2015. Hydrodynamics and sediment dynamics in a ice-covered tidal flat. In: Coastal Sediments 2015. World Scientific, 14 p. doi:10.1142/9789814689977_0083

Such processes under ice have mainly been studied in rivers, generally with stable water depth of several meters (e.g., Attar and Li 2012, Milburn and Prowse 2002). There has also been some work in nearshore areas, e.g. Morse et al. (2006) measuring and modelling tidal flow in a small estuary. However, studies in intertidal areas are scarcer, mainly because of the difficulty of measurements below moving ice cover. Dale et al. (2002) measured a few velocity profiles in Frobisher Bay (Baffin Island, Canada). Staats et al. (2001) monitored the Ems Estuary monthly for suspended particulate matter (SPM), including periods of thin ice cover (0.04-0.06 m) with lower SPM values. Although marsh sedimentation in the St. Lawrence is dominated by winter processes, these processes are poorly understood and the respective contributions of sediment transport by current and ice rafting have not been determined so far.

The objective of this study is to characterize currents, turbulence, and suspended sediment transport across an ice-covered intertidal zone. The aim is to better understand sediment transport by currents in winter and its importance relative to ice-rafting in tidal flats in the St. Lawrence Estuary.

Study Location and Methods

The Sacré-Coeur tidal flat and marsh are located west of Rimouski (Quebec) on the southern shore of the lower St. Lawrence Estuary (Fig. 1). The intertidal zone is ~1.3 km wide. A high marsh is separated from a low marsh with sparse *Spartina alterniflora* by a marsh scarp. Seaward is a 900-m wide tidal flat without prominent creeks, but with scattered boulders and cobbles. The area is partially protected against waves by two islands (St. Barnabé Island and Canuel Island). In winter, the ice foot is firmly attached to the high marsh during 2-3 months. The 0.5-m thick land-fast ice, which covers the low marsh and tidal flat, moves up and down with each tide. The extent of the land-fast ice varies during winter depending on temperature and wave action. Most of the above-ground vegetation of the low marsh disappears in winter. Surface salinity is 20-30 and the spring tidal range is 4.8 m.

Four ADV current meters (Nortek Vector) and two ADCPs (Nortek Aquadopp Profiler 2 MHz) were used to measure currents under ice on three days with different tidal heights in February 2013 (Table 1). Suspended sediment concentration (SSC) was measured with 5 OBSs (models OBS3 and OBS3+) that were connected to the ADVs and ADCPs. The instruments were distributed at five sites along an 800-m cross-shore transect from the low marsh to the outer tidal flat: site A at 100 m from marsh scarp, site B at 300 m, site C at 500 m, site D at 700 m, and site E at 870 m (Fig. 1, Table 1). Holes were cut through

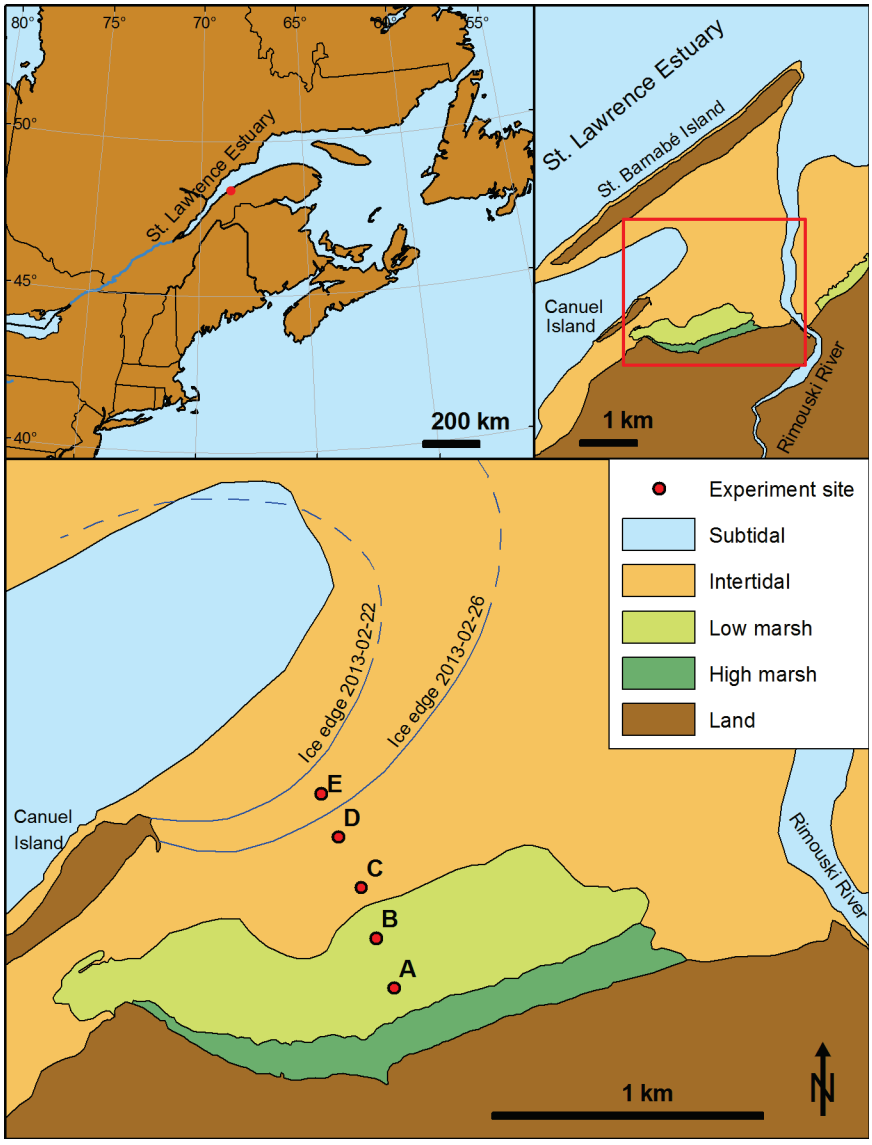

Fig. 1. Positions of the experiment sites on the Sacré-Coeur tidal flat and marsh with also extent of land-fast ice on the 22nd and the 26th February 2013

the 50-65-cm thick ice and instruments were suspended from the ice (Fig. 2), except for the ADV at site A, where a lateral foot maintained a fixed height of 0.10 m above bed. At each site an additional hole was cut to install a tide

Fig. 2. A) Structure supporting the head of the ADV with the electronic housing on the ice; at the back ADCP with support structure. B) Structure supporting the ADCP

ruler (for information during field work) and a tide gage resting on the ground (RBR TWR-2050).

Vertical ADV positions were regularly readjusted to maintain the sampling volume at 5-15 cm above bed. However, due to the difficulty of knowing the exact water height above bed at the ADV position from the nearby tide ruler, ADVs were sometimes measuring in the sediment or at the ADV weak-spot, the zone about 0.20 m above ground were the ADV produces a high turbulence artefact (Nortek 2005). The ADVs were recording bursts of 580 s at 16 Hz every 600 s with a nominal velocity range of ±0.3 m/s. The periods influenced by vertical instrument repositioning and when ADVs were measuring in the sediment were rejected. The period when ADVs measured at the weak spot were rejected for computation of turbulence kinetic energy (TKE). Mean velocity and TKE were then computed on 15-s intervals. ADV measurements with a correlation (quality index of measurement) lower than 70 % (generally in the weak spot) were rejected for the TKE computation, and TKE was not computed for 15-s intervals with less than 70% valid measurements.

The ADCP at site C (experiment 1) and at site B (experiments 2 and 3) measured 0.025 m cells for a total length of 1 m at 1 Hz in pulse coherent (PC) mode. The PC mode produces a weak spot zone like an ADV at about 1 m from

the bed (Nortek 2008). Data from this zone were rejected (Fig. 6). Records were then averaged over 1-minute intervals. The ADCPs at site E (experiment 2) and at site D (experiment 3) measured 0.1 m cells averaged over 580 s every 600 s (horizontal precision 0.014 m/s). For the ADCP at site B, boundary layer parameters z_0 (roughness length) and u_* (shear velocity) were computed from adequate semi-log profiles using the law of the wall; and u_* was converted to bed shear stress (τ_0). These parameters were computed for the lower boundary at the bed (τ_{bed}) and for the upper boundary at the bottom of the ice (τ_{ice}).

Results

Time-series of velocity and turbulence

Currents and turbulence were strongest when the incoming tide started to lift the ice from the ground, where it rested at low tide (Fig. 3-5). Currents then decreased toward slack water, and increased again with the ebb tide, reaching

Table 1. Tidal range and instrument* positions for the three experiments in February 2013

	1	**2**	**3**
Experiment	**February 11**	**February 22**	**February 26**
Tidal range**	4.30 m	2.06 m	3.67 m
Max. water depth at site C	2.61 m	1.42 m	2.19 m
Instrument at site A	–	ADV[a]	ADV[a]
Instrument at site B	–	ADV[a] + ADCP[a]	ADV[a] + ADCP[a]
Instrument at site C	ADV[a] + ADCP[a]	ADV	ADV[b]
Instrument at site D	–	ADV[b]	ADV + ADCP[a]
Instrument at site E	–	ADCP[a]	–

* ADVs are Nortek Vector, ADCPs are Nortek Aquadopp Profiler 2 MHz. A tide gage RBR TWR-2050 was also at each site.

** Recorded at the tide gage of the Canadian Hydrographic Service in the harbor of Rimouski.

[a] With turbidity sensor OBS3+.

[b] With turbidity sensor OBS3.

higher values at the seaward sites. Currents were slower at the landward sites. At spring tide (experiments 1 and 3), flood currents reached 0.2-0.3 m/s at the seaward sites and the ebb currents were a little slower (0.1-0.2 m/s). At neap tide (experiment 2) currents were gentler, with maxima of 0.1-0.2 m/s at the seaward sites. A very slow current is observed at the initial flooding at site C during experiment 3 (Fig. 5), but is not shown by the ADCP data (Fig. 6). This may be an artefact of an ADV positioned too high in the hole in the ice.

The flood current is directed toward the shore during the rising tide (between 145° and 250°), rotating slowly from SSE to SW (not illustrated). The ebb current is toward offshore (between 320° and 70°), rotating slowly clockwise during experiments 1 and 2, and counter-clockwise during experiment 3.

Very strong currents with high turbulence were often observed visually just when the rising tide reached the instrument holes. At this moment, water is pushed with high pressure through the narrow space between the bed and the ice, until the land-fast ice starts to float. Unfortunately, these currents could not be measured because the Vector ADV measures currents at 0.15 m from the probe, i.e. the water level must be 0.15 m above sampling volume. In contrast, currents slower than 0.02 m/s were sometimes recorded at low water heights when the ice hindered the water flow, e.g. at site A during experiment 2 (neap tide) or site C at the start of experiments 1 and 3.

The changing ADV height above the bed (lower panel on Fig. 3-5) must be taken into account when interpreting the current and turbulence data of the ADVs. Some current variations, like the repeated oscillations at site D at the end of experiment 3 (Fig. 5), are directly linked to the combination of vertical ice movements and repeated adjustments of the ADV position relative to the ice. Turbulence measurements are more likely to be influenced by ADV problems than mean velocities. Therefore, some high TKE measurements may due to instrument artifacts, even if we took care to validate the data quality.

Turbulence represented by TKE followed the same pattern as currents, with a decrease during slack water and generally higher TKE at the seaward sites (Fig. 3-5). TKE was also lower at neap tide (up to 0.6 Pa, experiment 2) than at spring tide (up to 1.0 Pa). However, some high TKE peaks exist just after flooding at sites B and D during experiment 2, at falling tide at site A during experiment 2, and just before high water at site B during experiment 3. This may be due to either uncommon, strong turbulent eddies produced between the bed and ice, or some undiagnosed instrument artefact.

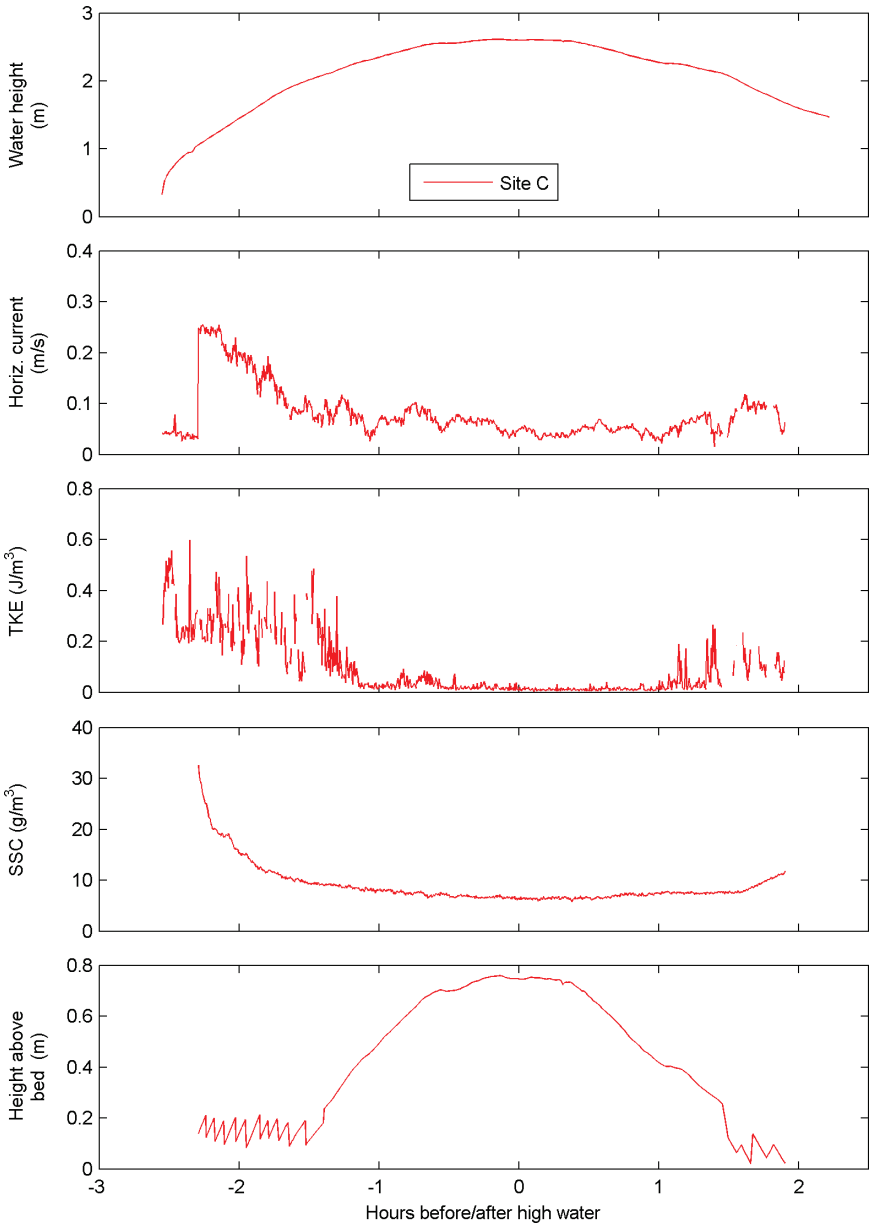

Fig. 3. Time-series of experiment 1 with water level, mean horizontal velocity, turbulent kinetic energy, suspended sediment concentration and height of the ADV sampling volume above bed

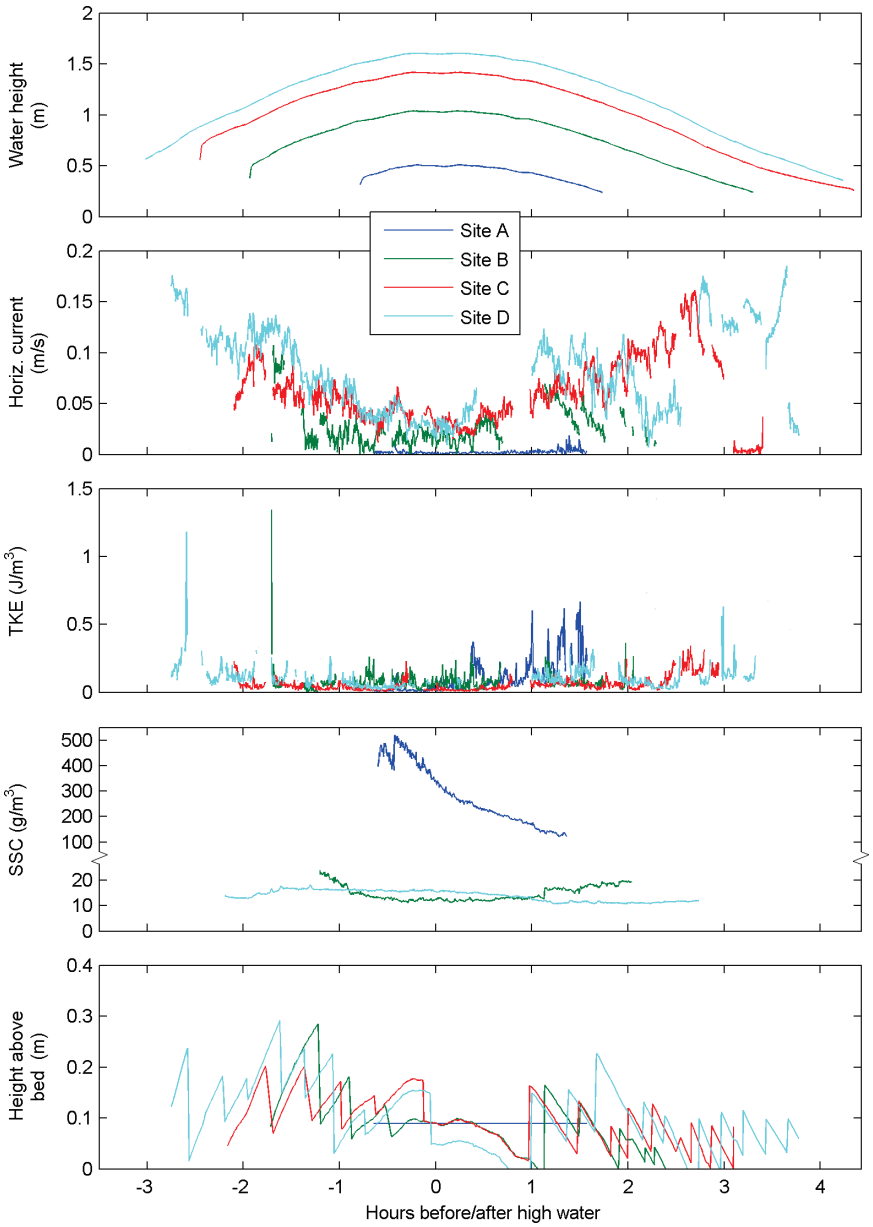

Fig. 4. Time-series of experiment 2 with water level, mean horizontal velocity, turbulent kinetic energy, suspended sediment concentration and the height of the ADV sampling volume above bed. SSC was not measured at location C

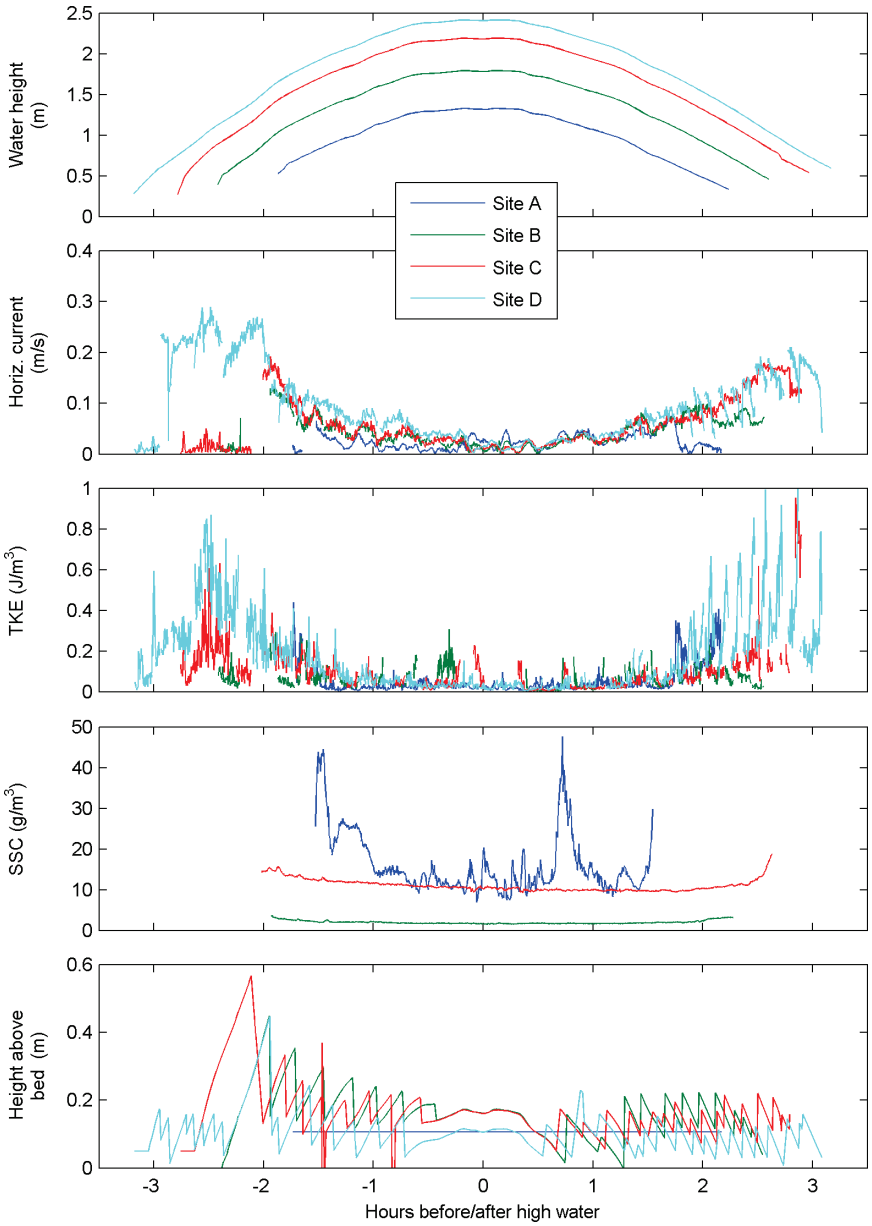

Fig. 5. Time-series of experiment 3 with water level, mean horizontal velocity, turbulent kinetic energy, suspended sediment concentration and height of theADV sampling volume above bed. SSC was not measured at location D

Velocity profiles

The ADCP recorded strong currents at initial flooding until the bed-ice distance reached 0.5 m at site B during experiment 3 (Fig. 6b). Afterward currents were weaker, and minimal around high water. These data also highlight the presence of many current pulses of 5-15 minutes, especially at lower velocities. The velocity profiles show two boundary layers, one near the bed, and the second at the water-ice interface, which both are generally logarithmic shaped (Fig. 6d).

The shear stresses at the bed (τ_{bed}) and at the ice bottom (τ_{ice}) follow the same pattern as the currents, i.e. maximum at flooding, decreasing afterward, and relatively high values during ebb tide (Fig. 6c). However, τ_{bed} could not be computed when the ADCP range did not reach the bed, and many upper boundary layer profiles around high water did not have a characteristic logarithmic shape, not allowing the computation of τ_{ice}. Therefore, shear stresses are not well defined ±1 hours from high water. τ_{bed} is stronger than τ_{ice}, with maximum values of 0.7 Pa and 0.27 Pa, respectively, at site B during experiment 3.

At the low marsh site B, the roughness length z_0 of the bed varied between 1 and 12 mm, which corresponds to an irregular bed surface or the presence of some sand ripples (Soulsby 1983), but this is much smaller than the roughness usually produced by marsh vegetation (Neumeier and Amos, 2006). The roughness length z_0 of the ice bottom varied between 1 and 14 mm. This variability depends of the ice bottom roughness in the upstream direction, which varies over a tidal cycle.

SSC

SSC was highest at the beginning of the flood and generally decreased toward slack water, with a slight increase sometimes during ebb tide (Fig. 3-5). SSC was also higher in the low marsh compared to the tidal flat, probably because the finer low-marsh sediments could be more easily resuspended. SSC was higher during experiment 2 than during experiments 1 and 3. This is surprising because experiment 2 was during neap tide whereas the two others had a larger tidal range and stronger currents. One possible explanation is that the narrower space between bed and ice at neap tide increases resuspension. In addition, the resuspended sediment would be diluted in a smaller water volume due to the smaller tidal prism. Another possibility is a SSC difference in the water brought to the intertidal zone by the tide, due to sediment resuspension in nearshore areas.

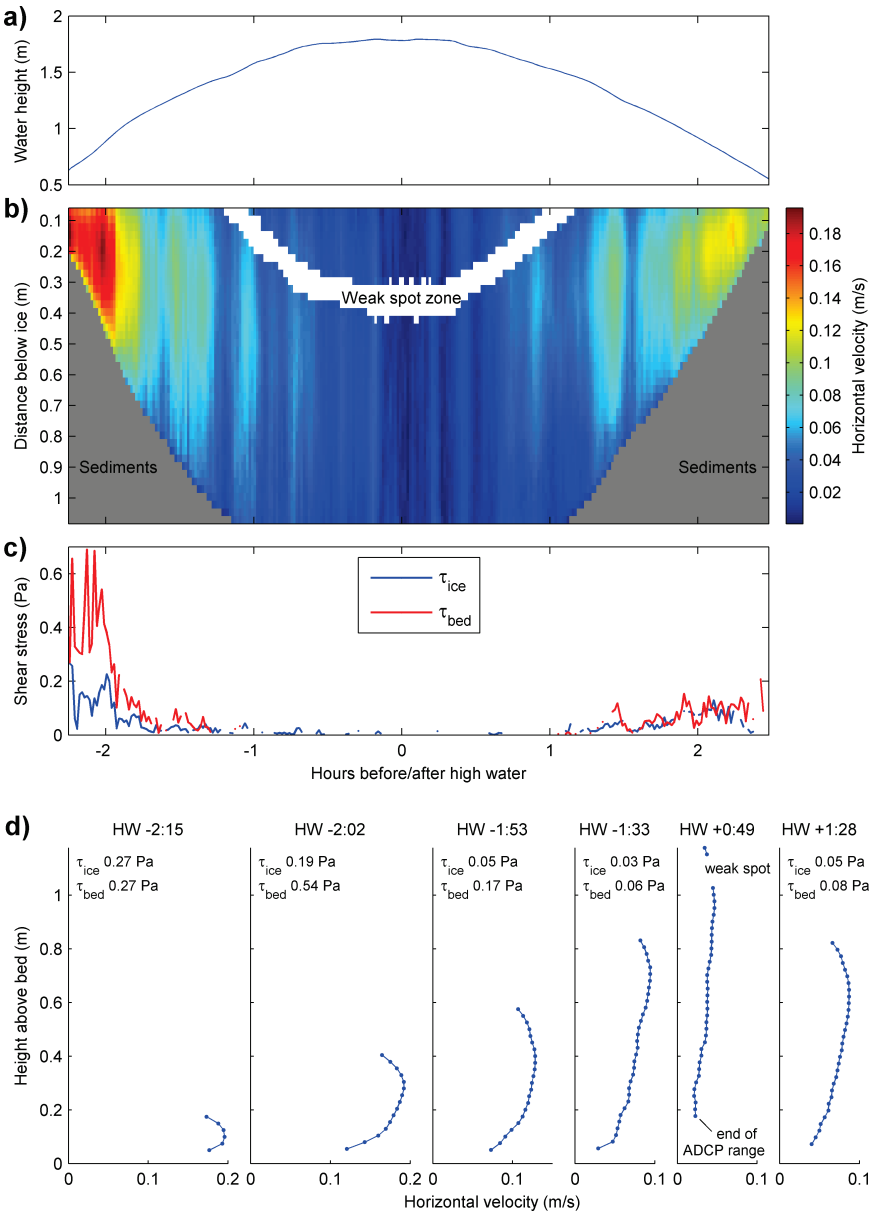

Fig. 6. ADCP results at site B during experiment 3. a) Water level measured with the tide gage. b) Horizontal velocity measured by the ADCP looking downward from the ice base; a weak spot zone occurs at about 1 m from the bed, which is blanked out. c) Shear stress at the ice bottom (upper boundary) and at the bed (lower boundary). d) Examples of profiles of horizontal velocity

Waves were not measured in front of the study area, but wave records exist at 32-m water depth for Saint-Ulric, located 75 km northeast on the south shore of the St. Lawrence Estuary (Neumeier and Joly 2014). There was a nearly continuous ice cover on 10 and 11 February (experiment 1), but no or minimal waves. One day before experiment 2, on 21 February 2013, there was a major storm from the northeast, with a significant wave height (H_{m0}) of 3.16 m and mean period T_{02} of 6.1 s. On 22 February, H_{m0} was about 1 m. The following days until experiment 3, H_{m0} was between 0.2 and 0.5 m.

The storm that arrived just before experiment 2 may explain the higher SSC measured on 22 February at sites B, C, and D. The very high SSC at site A (up to 400 g/m^3) is probably due to the very constricted water flow in this area that day.

Discussion

We measured velocity profiles with two boundary layers, at the bed and at the ice bottom, under land-fast ice, which were similar to those reported for ice-covered rivers and channels (e.g., Milburn and Prowse 2002; Atter and Li 2012). The ice presence and the absence of vegetation canopy push the current closer to the bed compared with ice-free conditions. Nevertheless the turbulence in the bed boundary layer is similar or lower than observed in marshes during the ice-free season. For example, Coulombier et al. (2012) measured much higher TKE (up to 16 J/m^3) in summer at another St. Lawrence marsh located 18 km away. These high summer values may be due to the roughness produced by the vegetation, or the presence of waves. Both vegetation and waves were absent under the land-fast ice.

We could not measure the strongest currents, which occur at flooding when water is pushed with pressure between the bed and ice resting on the bed. In this situation significant sediment resuspension and scour are likely to occur. SSC generally follows tidal current intensity. The comparison between experiment days shows that the SSC level is additionally controlled by storms resuspending sediments in nearshore ice-free waters. Very high sediment resuspension was observed on the low marsh at site A, much higher than is commonly measured on marshes in summer. This may be explained by the absence of protective vegetation canopy. Cohesive marsh sediments are usually also stabilized by biofilms, but the cold temperature and the absence of light under the ice probably reduce the presence of biofilms in winter.

The sampling volume of the ADVs could not always be maintained 5-15 cm above bed, because of the fast rise and fall of the ice with the tide, and the difficulty of knowing the exact ADV-bed distance under the ice cover.

Therefore the results must be interpreted with caution. Nevertheless this constitutes a unique dataset revealing the conditions below land-fast ice.

Conclusion

The temporal and lateral current variations correspond to the usual intertidal pattern: strong flood currents that slow down near high water, currents increasing again to medium strength during ebb tide, decreasing current magnitude from seaward to landward sites. However, the strongest currents occurred when water was pushed with high pressure under the ice resting on the ground. Velocity profiles show currents decreasing downward near the bed, but also upward near the water-ice interface. This may reduce the total flow, but can also push the velocity maximum toward the bed. Nevertheless, bed shear stress was lower than measured in summer marsh experiments, probably because of the absence of waves and vegetation canopy. Even if conditions on land-fast ice seem calm with minimal movements, significant sediment transport occurs below, which is amplified by the absence of marsh vegetation and probably also by reduced biofilm stabilization.

These experiments demonstrated the feasibility of measuring hydrodynamic conditions under land-fast ice. Data processing highlighted the importance of positioning the ADV correctly relative to the bed, in order to obtain easily interpretable results.

Acknowledgements

Bruno Cayouette, Sylvain Joly, Eliott Bismuth, and Dany Dumont assisted with field work. This research was funded by the Canadian Foudation for Innovation.

References

Attar, S. and Li, S.S. (2012). "Data-fitted velocity profiles for ice-covered rivers," *Canadian Journal of Civil Engineering*, 39, 334-338.

Barnhart, K.R., Overeem, I., Anderson, R.S. (2014). "The effect of changing sea ice on the physical vulnerability of Arctic coasts". *Cryosphere*, 8, 1777-1799.

Dale, J. E., Leech, S., McCann, S. B., and Samuelson, G. (2002). "Sedimentary characteristics, biological zonation and physical processes of the tidal flats of Iqaluit, Nunavut," In: "*Landscapes of transition*, " Hewitt, K., Burne M.-L., English, M., and Young G. (eds.). Kluwer, 205-234.

Coulombier, T., Neumeier, U., and Bernatchez, P. (2012). "Sediment transport in a cold climate salt marsh (St. Lawrence Estuary, Canada), the importance of vegetation and waves," *Estuarine, Coastal and Shelf Science*, 101, 64-75.

Milburn, D., and Prowse, T.D. (2002). "Under-ice movement of cohesive sediments before river-ice breakup," *Hydrological Processes*, 16, 832-834.

Morse, B., Ringô, B., Messier, D., Thanh-Quach, T., and Stander, E. (2006). "Hydrodynamics of mesotidal estuary in winter," *Journal of Cold Regions Engineering*, 20, 95-115.

Neumeier, U., Amos, C.L. (2006). "The influence of vegetation on turbulence and flow velocities in European salt-marshes," *Sedimentology*, 53, 259-277.

Neumeier, U. (2011). "Boulder transport by ice on a St. Lawrence salt-marsh, pattern of pluriannual movements," *Proceedings Coastal Sediments '11*, World Scientific Publishing, 2533-2545.

Neumeier, U., Joly, S. (2014). "*Mesures des vagues, des courants et des glaces de 2010 à 2014 dans l'estuaire et le golfe du Saint-Laurent pour les problèmes d'érosion côtière*," Report for the Ministère de la Sécurité publique du Québec, Institut des sciences de la mer de Rimouski, Rimouski, QC, 98 p.

Nortek (2005). "*Vector Current Meter, User Manual,*" Nortek AS, 84 p.

Nortek (2008). "*Aquadopp High Resolution, User Manual,*" Nortek AS, 37 p.

Soulsby, R.L. (1983). "The bottom boundary layer of shelf seas". In: Johns B. (ed.) "*Physical Oceanography of Coastal and Shelf Seas*", Elsevier, 189-266.

Staats, N., de Deckere, E., Kornman, B., van der Lee, W., Termaat, R., Terwindt, J., and de Winder, B. (2001). "Observations on suspended particulate matter (SPM) and microalgae in the Dollard Estuary, The Netherlands: Importance of late winter ice cover of the intertidal flats," *Estuarine, Coastal and Shelf Science*, 53, 297-306.

Troude, J. P., Sérodes, J. B. (1988). "Le rôle des glaces dans le régimee morpho-sédimentologique d'un estran de l'estuaire du Saint-Laurent," *Canadian Journal of Civil Engineering*, 15, 348-354.